

Article

An In-Depth Exploration of Numerical Simulations for Stress Fields in Multi-Directional Rolling Processes

Lele Sun ^{1,*} , Mingbo Zhang ² and Changxu Xu ³

¹ School of Mechanical Science and Engineering, Huazhong University of Science and Technology, Wuhan 430074, China

² School of Materials Science and Engineering, Huazhong University of Science and Technology, Wuhan 430074, China

³ School of Aerospace Engineering, Huazhong University of Science and Technology, Wuhan 430074, China

* Correspondence: d201880273@hust.edu.cn; Tel.: +86-278-7543-493

Abstract: To address issues such as large surface roughness, coarse grains, and poor mechanical properties in low-carbon steel parts produced through wire arc additive manufacturing (WAAM), this paper proposes a method combining multi-directional incremental forming with the WAAM process. The additive manufacturing and cooling processes were simulated using the finite element software Abaqus to analyze the effects of multi-directional additive manufacturing on the stress field of the fabricated parts. The results indicate that after multi-directional incremental forming, the residual stress in the fabricated parts shifts from tensile stress to compressive stress, thereby reducing the risk of defects such as cracks. Moreover, the equivalent plastic strain of the processed parts increases, and the surface microhardness improves, with the most significant impact of multi-directional incremental forming observed in the contact area of the rolling head.

Keywords: wire arc additive manufacturing; multi-directional incremental forming; residual stress; surface mechanical properties; process parameters



Citation: Sun, L.; Zhang, M.; Xu, C. An In-Depth Exploration of Numerical Simulations for Stress Fields in Multi-Directional Rolling Processes. *J. Manuf. Mater. Process.* **2024**, *8*, 229. <https://doi.org/10.3390/jmmp8050229>

Academic Editor: David L. Sales

Received: 22 August 2024

Revised: 2 October 2024

Accepted: 6 October 2024

Published: 12 October 2024



Copyright: © 2024 by the authors. Licensee MDPI, Basel, Switzerland. This article is an open access article distributed under the terms and conditions of the Creative Commons Attribution (CC BY) license (<https://creativecommons.org/licenses/by/4.0/>).

1. Introduction

Additive manufacturing (AM) [1] technology is an emerging digital three-dimensional (3D) solid manufacturing method, also known as “Rapid Prototyping” or “3D Printing” (3DP). Unlike traditional material-forming methods such as subtractive machining and forging, AM technology overcomes the limitations of conventional subtractive manufacturing techniques. Its layer-by-layer printing process, based on a digital 3D model of the part, introduces revolutionary flexibility in design and manufacturing [2]. It allows the rapid and direct formation of complex structural components that are difficult to produce using traditional manufacturing techniques, making it widely applicable in fields such as aerospace, submarines, ships, energy, and healthcare.

Based on different material supply forms, metal additive manufacturing technology can be divided into two major categories: Powder Bed Fusion (PBF) and Direct Energy Deposition (DED). According to the type of heat source, these technologies can be further categorized into three types: those using laser, electron beams, and arcs. Powder Bed Fusion technology mainly includes Selective Laser Melting (SLM) [3], Laser Engineering Net Shaping (LENS) [4], and Electron Beam Selective Melting (EBSM) [5]. Direct Energy Deposition technology mainly consists of Electron Beam Solid Freeform Fabrication (EB-SFF) [6], where the material is changed from powder to synchronously delivered metal wire, and wire and arc additive manufacturing (WAAM) [2].

In contrast, arc additive manufacturing technology, which utilizes plasma arcs and electric arcs as high-energy beam heat sources, has been attracting increasing attention from researchers. It originated from Shielded Metal Arc Welding (SMAW) technology in the early 20th century, patented by Baker [7], which employed the method of melting electrode

gas-shielded welding for layer-by-layer deposition. This technology offers significant advantages in forming size, efficiency, material utilization, cost, and applicability. It enables the integrated additive manufacturing of large and complex components, making it a key development direction for modern green manufacturing and low-carbon, high-efficiency industries [8]. This technology primarily evolved from three mainstream welding techniques: Gas Metal Arc Welding (GMAW), Gas Tungsten Arc Welding (GTAW), and Plasma Arc Welding (PAW). It can also be used to upgrade the existing welding industry [9].

To address the issues of suboptimal morphology quality and poor metallurgical performance in formed parts, researchers have combined various manufacturing principles with arc additive manufacturing technology, resulting in several derived types: (1) The combination of arc deposition and subtractive mechanical processing leverages the high precision and broad processing range of milling [10,11], achieving high-precision and high-efficiency manufacturing of metal formed parts. (2) The combination of arc deposition with "isomaterial" manufacturing principles such as rolling [12,13], forging [14,15], and shot peening [16,17] introduces mechanical force fields to the deposited layers during forming or post-processing stages, inducing plastic deformation, improving grain morphology, and regulating microstructure. This enhances the mechanical properties and, to some extent, the geometric accuracy of the formed parts. (3) The combination of arc deposition with special energy fields such as ultrasound, electromagnetic [18], and laser energy throughout the entire forming process improves the morphology and microstructure of the formed parts.

In the field of combined manufacturing processes involving additive manufacturing and rolling, research on residual stress and plastic strain is limited. This paper employs the finite element method to couple the additive manufacturing of low-carbon steel with longitudinal and transverse rolling processes. The rolling force is utilized to induce significant compressive plastic deformation in the metal's surface layer. A comparative analysis of the stress fields before and after rolling the additive parts is conducted. This provides a theoretical basis and reference for synchronous longitudinal and transverse rolling.

The innovations of this paper include the following:

- (1) Multi-directional rolling study: Previous research on the combination of additive manufacturing and rolling has been limited to unilateral rolling. This study is the first to simulate both longitudinal and transverse rolling, thereby filling a gap in this field.
- (2) Stress field analysis: This paper provides a detailed comparison between numerical simulations and measured residual stresses, offering a theoretical basis and reference for the formation of specific parts in future additive manufacturing processes, which has significant practical value.
- (3) Combination of simulation and measurement: By integrating simulation and measured data, the research results become more objective and realistic, enhancing this study's credibility and scientific validity, thereby demonstrating methodological innovation.

The main content includes the establishment of the finite element model in the Section 2; stress field and measurement validation in the Section 3; and conclusions and prospects in the Section 4.

2. Materials and Methods

In arc additive manufacturing, rapid deposition rates are typically accompanied by high heat input and poor molten pool stability, often resulting in reduced dimensional accuracy and mechanical properties of low-carbon steel components. The rolling process can enhance the forming quality of the parts and improve their microstructure and mechanical properties. This section focuses on low-carbon steel, utilizing the finite element software Abaqus 2021 to conduct numerical simulations of the stress field in multi-directional rolling forming processes.

2.1. Finite Element Model of Multi-Directional Rolling Forming

Based on the actual multi-directional rolling forming process, this paper establishes a finite element model for multi-directional rolling-formed additive components. The

substrate dimensions are $140 \times 40 \times 14 \text{ mm}^3$, and the dimensions of the single-pass multi-layer straight wall after stacking are $100 \times 8 \times 14 \text{ mm}^3$. The forward roller has a diameter of 24 mm, while the lateral roller has a diameter of 40 mm. The forward roller maintains a distance of 40 mm from the heat source, while the lateral roller maintains a distance of 20 mm. The forward and lateral rollers feed synchronously with the heat source at a speed of 400 mm/min (6.6 mm/s). Figure 1 shows the finite element model of the multi-directional rolling-formed additive components, which uses first-order hexahedral elements with eight nodes. After meshing, the finite element model contains 95,782 nodes and 80,324 elements, with uniform mesh quality that meets the requirements of finite element analysis. As shown in Figure 1, in the formed part printed along the weld bead direction, the x -direction represents the weld bead direction, the y -direction represents the width of the weld bead, and the z -direction represents the height of the accumulated layers.

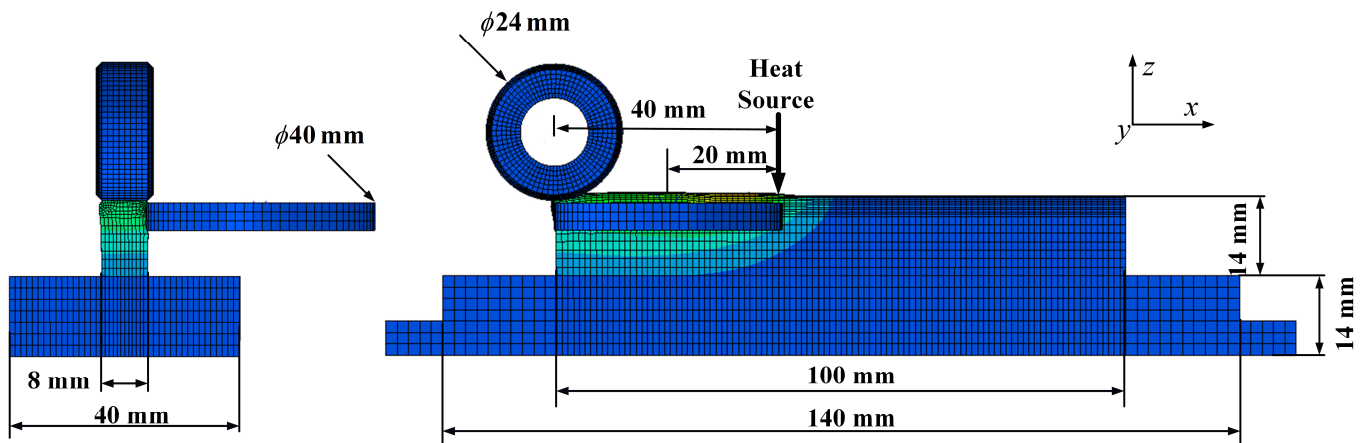


Figure 1. Finite element model of multi-directional rolling-formed additive parts.

2.2. Heat Source Settings

During the arc additive manufacturing process, the material experiences rapid cooling and heating due to high thermal input, necessitating numerical simulations to account for the heat source distribution in the depth direction. During the forming stage, the movement of the heat source results in differing sizes of the molten and solidified zones before and after the heat source. Common welding heat source models include the concentrated heat source model, the plane heat source model, and the volumetric heat source model. In actual deposition forming experiments, the concentrated heat source model can be used if the heat source energy distribution has a minimal impact on the study area. However, in arc additive manufacturing, the energy density of the heat source is clearly non-uniformly distributed, making this model unsuitable for the finite element analysis of additively manufactured parts formed by multi-directional rolling. Additionally, the plane heat source model fails to account for the energy distribution in the depth direction of the molten pool, leading to significant calculation errors in arc additive manufacturing simulations. Considering the phenomenon where the arc crater exhibits a regular symmetric ellipsoidal shape when the arc is extinguished without filler during the actual deposition forming process, this paper adopts the double-ellipsoid heat source model, a type of volumetric heat source model, to describe the arc heat source for better alignment with actual experiments.

As illustrated in Figure 2, the double-ellipsoid heat source consists of two quarter ellipsoids. In this configuration, the long semi-axis of the ellipsoid in front of the heat source center is relatively short, whereas the long semi-axis of the ellipsoid behind the heat source center is comparatively long [19].

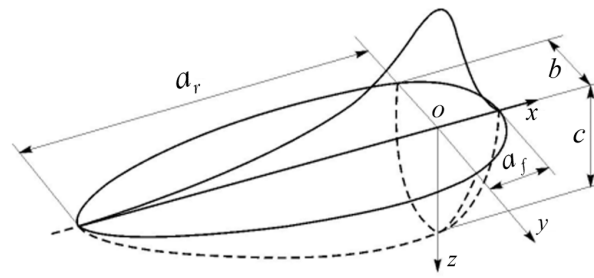


Figure 2. Schematic diagram of the double-ellipsoidal heat source model.

The distribution of heat sources is as follows:

$$\begin{cases} q_f(x, y, z, t) = \frac{6\sqrt{3}f_f Q}{\pi a_f b c \sqrt{\pi}} \exp\left[\frac{-3x^2}{a_f^2} + \frac{-3y^2}{b^2} + \frac{-3z^2}{c^2}\right], & x \geq 0 \\ q_r(x, y, z, t) = \frac{6\sqrt{3}f_r Q}{\pi a_r b c \sqrt{\pi}} \exp\left[\frac{-3x^2}{a_r^2} + \frac{-3y^2}{b^2} + \frac{-3z^2}{c^2}\right], & x < 0 \end{cases} \quad (1)$$

In the formula, a_f and a_r represent the major axes of the front and rear ellipsoids, respectively, measured in meters (m); q_f and q_r represent the heat flux densities of the front and rear ellipsoids, respectively, measured in W/m^2 ; b represents the minor axis of the front and rear ellipsoids, measured in meters (m); c represents the heat source depth, measured in meters (m); Q represents the heat input power, measured in watts (W); and f_f and f_r respectively represent the proportions of heat input for the front and rear ellipsoids. By adjusting based on comparisons with the actual weld pool depth and width, the values in this model are determined to be $a_r = 11$ mm, $a_f = 2$ mm, $b = 2$ mm, and $c = 1.5$ mm.

The loading method in this study discretizes the heat source movement into multiple spatial load steps. The simulation sequentially activates each heat source load during the movement, with the activation speed matching the actual welding speed of 6.6 mm/s.

2.3. Boundary Condition Setting

The numerical model of arc additive manufacturing involves two boundary conditions: the temperature field and displacement constraints. The initial temperature of the temperature field is set to room temperature, 20 °C (293 K). The boundary conditions for the temperature field involve establishing a heat transfer model on the substrate and weld bead surfaces. This study employs a composite heat transfer coefficient that comprehensively considers the combined effects of thermal radiation and convection [20], described as

$$h = \frac{\varepsilon_t \sigma_B (\theta^4 - \theta_0^4)}{(\theta - \theta_0)} + \alpha \quad (2)$$

The displacement constraint boundary conditions aim to restrict the rigid displacement of the substrate to prevent warping deformation. The setup of displacement constraints must ensure that the constraints in the numerical simulation match those of the substrate in the experiment, corresponding to the deformation of the formed sample. Additionally, the load in the numerical model is represented by a moving double-ellipsoid arc heat source, with a speed matching the actual welding speed of 6.6 mm/s.

2.4. Material Model

The forward and lateral rollers are made of quenched and hardened 45 steel, which possesses significantly higher hardness and strength compared to low-carbon steel. Since this study primarily focuses on the metal deposition layer, the deformation of the rollers during rolling is neglected. The rollers are treated as rigid bodies with discrete rigid body constraints applied. In the simulation, the contact between the forward and lateral

rollers and the weld bead is modeled as surface-to-surface contact, utilizing the penalty function contact algorithm with a Coulomb friction coefficient. Rotational constraints are imposed at the reference point of the rolling head, and its movement speed is set to 6.6 mm/s. During the arc additive manufacturing process, the temperature of the metal material varies significantly, and its thermophysical parameters change accordingly. Therefore, accurately setting the material property parameters is crucial for obtaining precise numerical simulation results. The materials used for the substrate and welding wire in this study are low-carbon steels, and the changes in their thermophysical parameters are illustrated in Figure 3 [21].

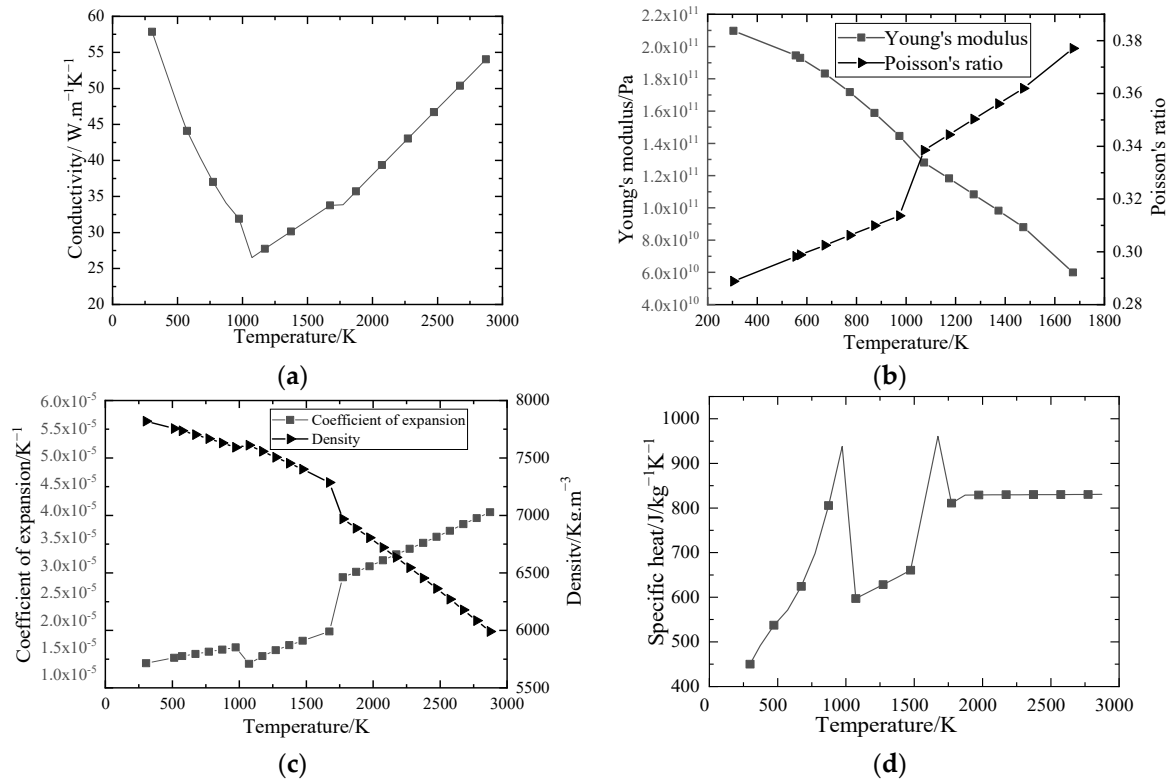


Figure 3. Relationship graph of some thermophysical properties of low-carbon steel with temperature changes. (a) The conductivity variation curve with temperature, (b) the curve of Young’s modulus and Poisson’s ratio with temperature variation, (c) the curve of the expansion coefficient and density with temperature variation, and (d) the curve of specific heat with temperature variation.

3. Stress Field Analysis

3.1. Analysis of the Stress Field Results in Free Deposition

During the multi-directional rolling forming process, the deposited layer transitions from a solid state to a molten state and then cools back to a solid state. These state transitions are accompanied by expansion and contraction, causing different parts of the deposited layer to be constrained by adjacent sections, thereby generating thermal stress. According to the von Mises criterion, or the fourth strength theory, when the material stress exceeds its yield strength, plastic deformation occurs, leading to reduced structural rigidity and stability.

To investigate the stress distribution during the free melting accumulation forming process, finite element numerical simulations were conducted on the formed parts in a free melting state. Figure 4 illustrates the distribution of residual stress in the surface material of the weld bead when the heat source is applied to the end point of the model. Under the influence of the heat source, the surface material of the weld bead underwent a heating process, followed by a cooling phase where it was constrained by the surrounding material, resulting in tensile stress in the surface material and ultimately forming the residual stress

distribution shown in Figure 4a. As shown in Figure 4a, the equivalent stress of the formed part predominantly exhibits a tensile stress state. The residual stress in the central region is relatively stable, with minor numerical fluctuations. However, at both ends, specifically the starting and ending points of the arc additive manufacturing, the distribution of residual stress is relatively unstable, exhibiting significant fluctuations. Figure 4b shows that there is significant residual tensile stress in the surface material of the weld bead in the x -direction. In contrast, the residual stresses in the y -direction and z -direction shown in Figure 4c,d are nearly zero. Therefore, it can be concluded that for arc additive manufacturing processes requiring stress improvement, the focus should primarily be on addressing the residual stress in the x -direction.

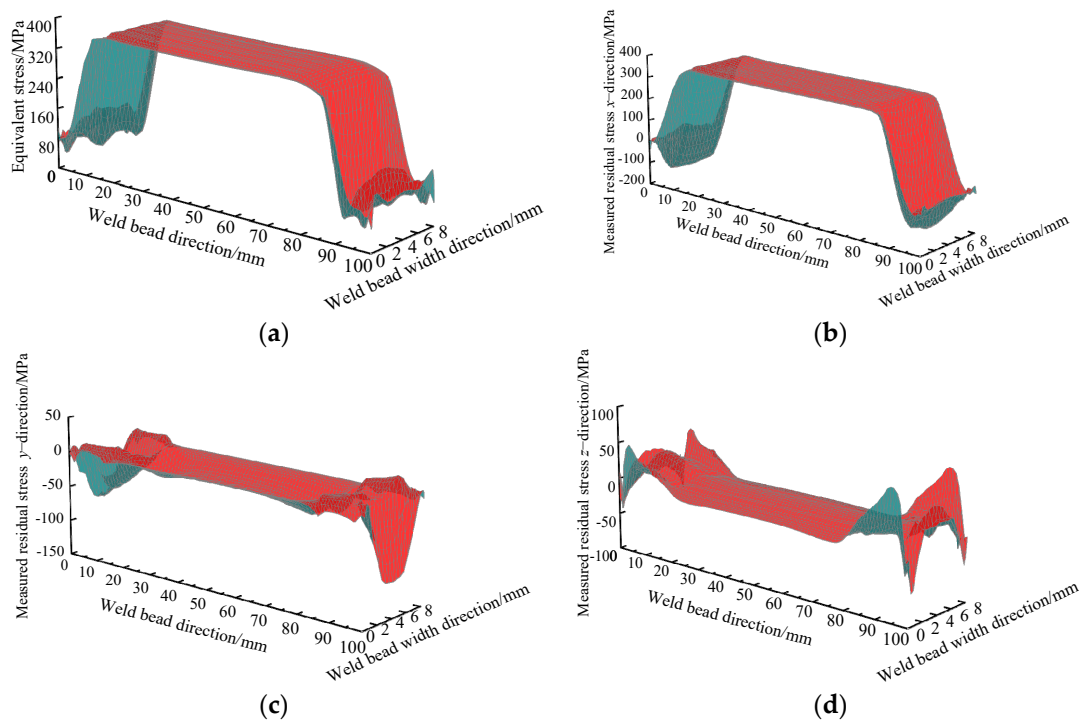


Figure 4. Stress distribution of weld pass surface material under heat source loading. (a) Equivalent stress, (b) measured residual stress in the x -direction, (c) measured residual stress in the y -direction, and (d) measured residual stress in the z -direction.

As illustrated in Figure 5, this study selected two paths, AB and CD, to further investigate the residual stress distribution of the formed part through stress field analysis. The dimensions of the single-pass, multi-layer straight-wall component are $100 \times 8 \times 14 \text{ mm}^3$, with path AB oriented opposite to the z -direction. Point A is situated at the midpoint of the 100 mm length of the formed component along the x -axis and at the midpoint of the 8 mm width of the weld bead along the y -axis. Point B is positioned at the junction of the weld bead and the substrate, 14 mm below Point A along the z -axis. Path CD is parallel to the x -direction of the weld formation, with Point C situated at the starting position of 100 mm along the x -axis of the coordinate system, and at the midpoint of the 8 mm weld width on the y -axis. Points 1, 2, and 3 represent three paths originating from the contact position between the weld and the substrate, selected at equal intervals upward from the bottom.

Figure 6 shows the distribution curves of each stress component in the AB direction. The results show that direction x exhibits a tensile stress state, while the stresses in the y -direction and z -direction are close to zero, with the stress in the z -direction being the smallest.

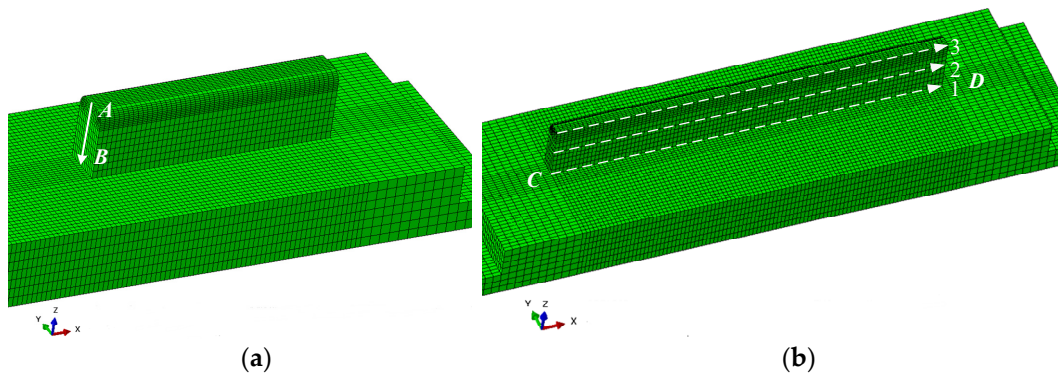


Figure 5. Definition of the directions for the two paths. (a) Direction of path AB, and (b) direction of path CD.

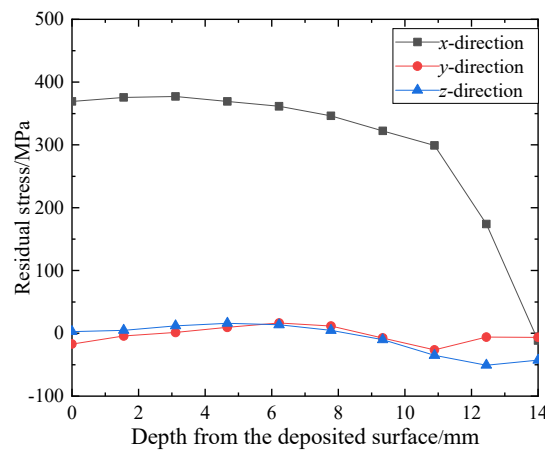


Figure 6. Distribution of residual stress in x -direction, y -direction, and z -direction under path AB.

Figure 7 illustrates the stress analysis in both the x - and y -directions for three equally spaced paths, chosen from the bottom upward along the CD direction. The x -direction exhibits a tensile stress state, with lower stresses at the start and end points, and a compressive state in the middle. The y -direction demonstrates compressive stress at the start and end positions for each layer, with relatively uniform stress values in the middle.

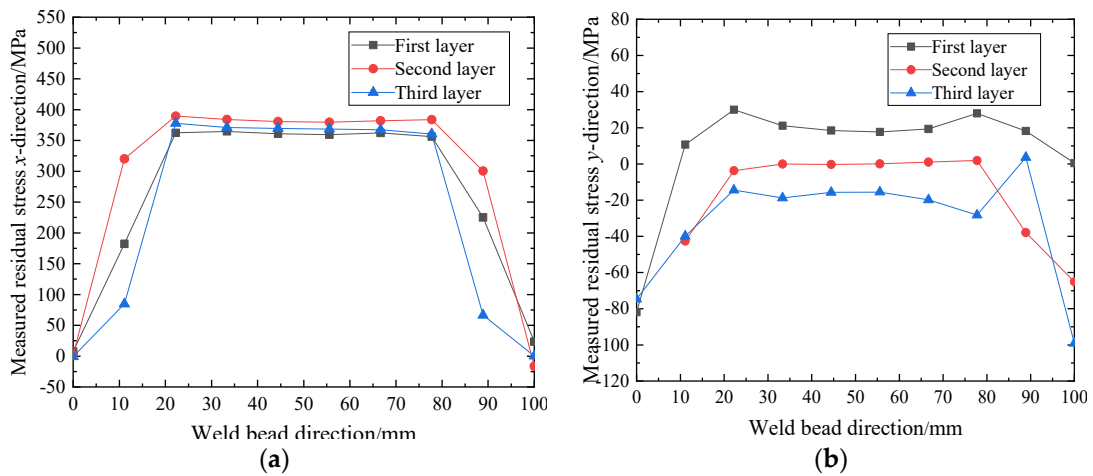


Figure 7. Residual stress distribution along direction CD. (a) Measured residual stress in the x -direction, and (b) measured residual stress in the y -direction.

3.2. Analysis of the Stress Field Results of the Forward Lateral Rolling Force

In the process of arc additive manufacturing, the results of the thermal stress field are taken as initial stress, and by adding forward and lateral rolling treatments, the stress field results are further analyzed. As shown in Figure 8, forward and lateral rolling are performed simultaneously with thermal source loading, with a forward rolling force set to 7.2 kN and a lateral rolling force set to 3 kN, corresponding to forward and lateral reduction amounts of 0.8 mm and 0.5 mm, respectively. After the forward and lateral rolling processes, the residual stress distribution of the weld bead surface material of the formed part changed significantly. After forward and lateral rolling, the residual tensile stress in the x - and y -directions on the weld bead surface of the formed part is reduced and transformed into beneficial compressive stress. This indicates that forward and lateral rolling can generate compressive stress in the weld bead surface material of the formed part, thereby improving the distribution of residual stress. The generation of this compressive stress helps to improve the processing quality of additive manufacturing parts and enhances their strength and toughness.

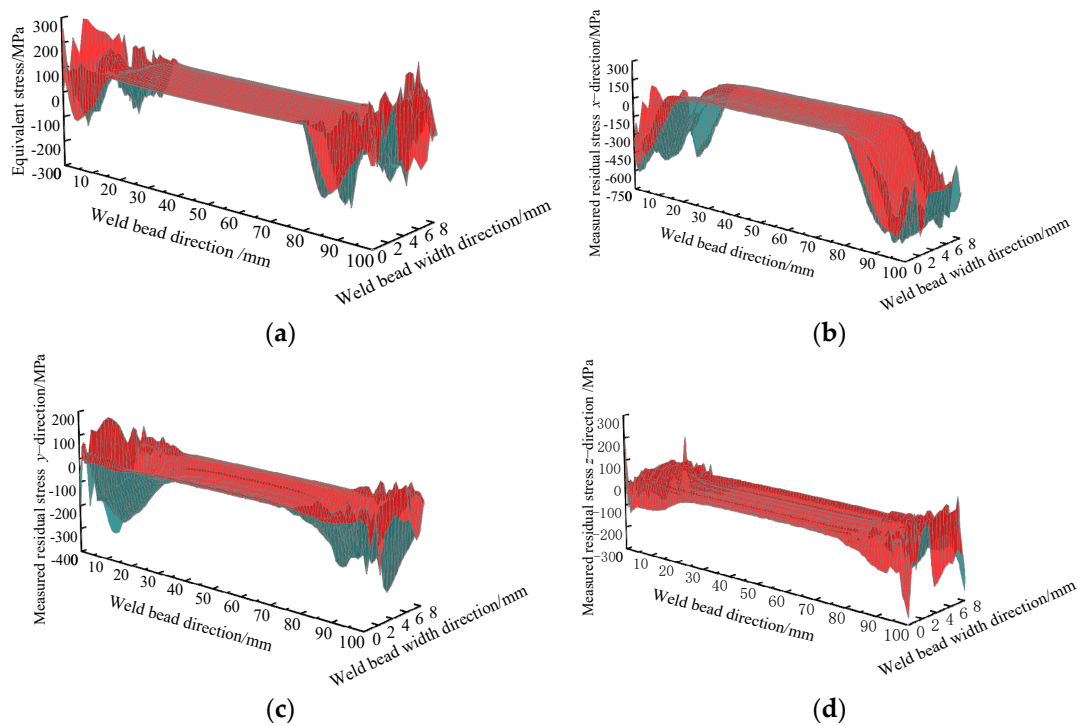


Figure 8. Stress distribution of weld pass surface material after multi-directional rolling: (a) equivalent stress, (b) measured residual stress in the x -direction, (c) measured residual stress in the y -direction, and (d) measured residual stress in the z -direction.

Upon completion of the forward and lateral rolling processes, two paths were selected to study the stress and strain distribution patterns of the formed part. The residual stress and equivalent plastic strain before and after rolling were analyzed, as illustrated in Figures 9 and 10.

Figure 9a shows that the rolled formed part initially exhibits residual compressive stress in the thickness direction, with a maximum value of -43 MPa. As depth increases, the residual compressive stress gradually transitions into tensile stress. At a depth of 13.3 mm from the surface, the residual stress value approximates the pre-rolling stress value. This indicates that the rolling effect has a specific depth range. With a forward rolling force of 7.2 kN and a lateral rolling force of 3 kN, the depth of influence is approximately 13 mm. Figure 9b shows that the equivalent plastic strain of the processed part gradually decreases with increasing depth, reducing to zero at approximately 10 mm. The equivalent

plastic strain is largest at the material surface, indicating that the rolling effect is greatest at the direct acting site and has a specific depth and range.

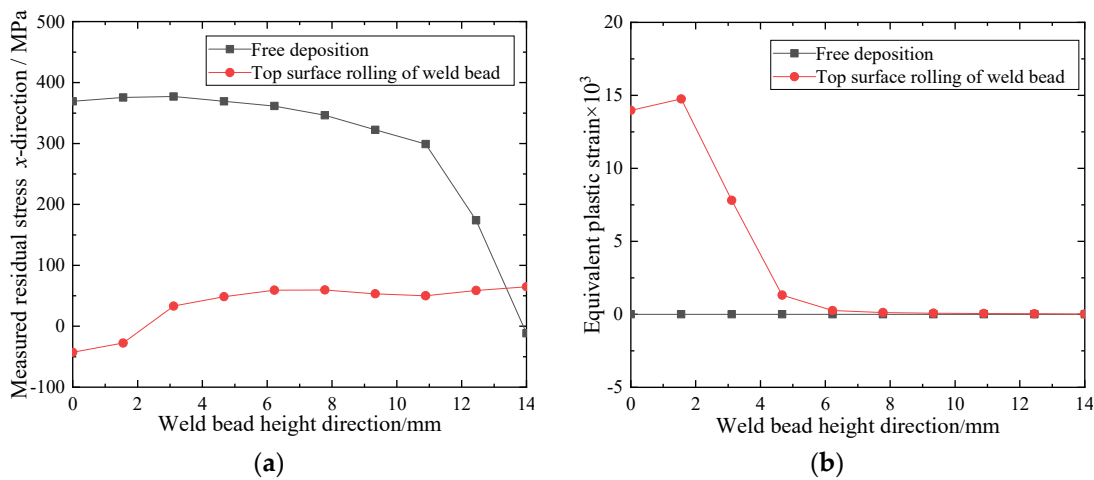


Figure 9. The curve of equivalent plastic strain and the residual stress in the x -direction distribution along path AB. (a) Measured residual stress in the x -direction, (b) equivalent plastic strain curve.

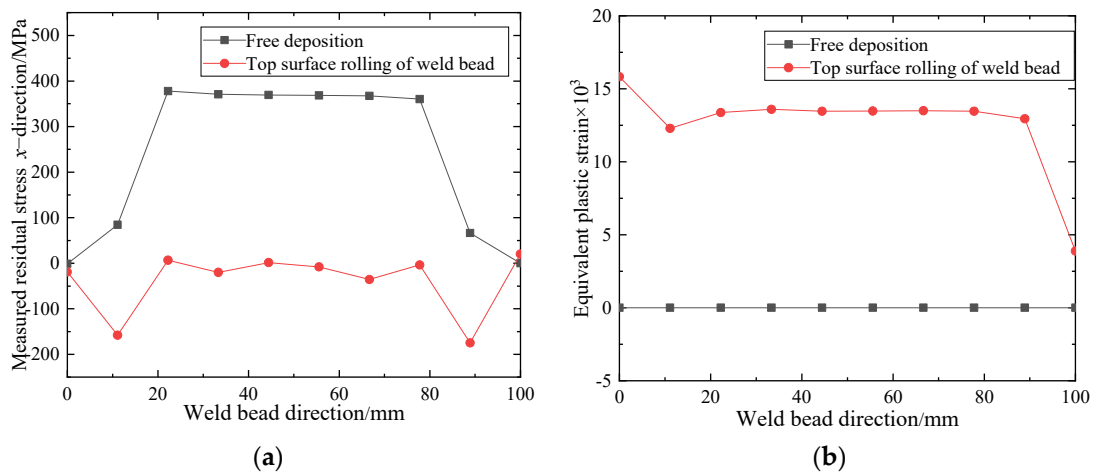


Figure 10. The curve of equivalent plastic strain and the residual stress in the x -direction distribution along path CD. (a) Measured residual stress in the x -direction, (b) equivalent plastic strain curve.

Disregarding the stress concentration caused by the model edge, Figure 10a illustrates that after forward rolling, the residual tensile stress in the x -direction on the surface of the formed part is converted into compressive stress. Before rolling, the average residual stress of the formed part was 317 MPa; after rolling, this value decreased to -62 MPa, representing a reduction of 119.6%. This result indicates that forward rolling can significantly reduce the risk of defects, such as cracks occurring perpendicular to the x -direction, thereby enhancing the reliability and service life of the formed part. Figure 10b shows that the equivalent plastic strain value on the surface of the formed part increases after rolling. Disregarding the high equivalent plastic strain values caused by stress concentration at the model edge, the equivalent plastic strain values of the formed part after rolling range from a maximum of 0.136 to a minimum of 0.123, with an average value of 0.133. This indicates a significant improvement in the surface microhardness of the formed part after rolling.

3.3. Validity Verification

In this paper, Q235 low-carbon steel, with a carbon content of no more than 0.20 wt%, is selected as the base material, while ER50-6 low-carbon steel wire with a diameter of

1.2 mm is chosen as the welding wire. The chemical composition of the materials is shown in Table 1. The substrate dimensions are 140 × 40 × 14 mm³. Before the experiment begins, to prevent substrate deformation or displacement during processing, a press block is used to secure it on the turntable.

Table 1. Chemical composition of substrate and wire (mass fraction, %).

Grade	C	S	Mn	Si	P	Cr	Ni	Mo	V	Al	Ti + Zr	Cu
Q235	≤1.8	≤3.0	3.5~6.5	≤0.4	≤0.4	---	---	---	---	---	---	---
ER50-6	0.80	0.13	15.5	9.0	0.18	0.34	0.15	0.02	0.01	0.05	0.06	1.34

The arc deposition manufacturing setup primarily includes a welding machine, welding gun with its supporting clamping mechanism, wire feeding machine, and protective gas cylinder, among other components. In this study, the German Lorich Mig welding machine V3 (LORCH Auenwald, Germany). is employed, which can accurately control voltage, current, wire feed speed, and protective gas flow parameters. Additionally, it enables external real-time control of arc start–stop through communication with the machine tool control cabinet, providing a robust process foundation for arc additive manufacturing.

To verify the effectiveness of the simulation, as shown in Table 2, the process parameters were set as follows: welding speed of 400 mm/min, wire feed speed of 6.5 m/min, arc length correction of 15, forward rolling reduction of 0.8 mm, and side rolling reduction of 0.5 mm. These parameters were used to print a single straight wall with a width of 8 mm and a height of 14 mm. It is important to note that during the forming process, the dirt and oxide on the surface of the bead should be cleaned after each layer of printing.

Table 2. Process parameters of arc additive manufacturing process.

Process Parameter	Numerical Value	Process Parameter	Numerical Value
Welding voltage (V)	22.8	Arc length (mm)	15
Welding current (A)	197	Wire diameter (mm)	1.2
Welding mode	Pulse	Duration of arcing (s)	0.6
Shielding gas	98%Ar + 2%CO ₂	Shutdown duration (s)	0.6
Air flow (L/min)	23 ± 1	Protection gas pre-flow time (s)	0.8
Wire feed speed (m/min)	6.5	Arcing current (A)	128
Welding speed (mm/min)	400	---	---

As shown in Figure 11, this study employs a Proto X-ray diffractometer, manufactured by Proto Company (Proto Manufacturing Ltd., Windsor, ON, Canada), to test the residual stress of single-channel straight-wall forming parts. In this context, the *x*-axis of the coordinate system denotes the forming direction of the weld bead, while the *y*-axis represents its width direction. The residual stress measured in the *x*-direction aligns with the forming direction of the weld bead. The testing method is as follows: Starting from position “1” on the weld surface in Figure 11a, which is 22 mm from the start of the weld, residual stress data are extracted every 11 mm along the forming direction of the weld (i.e., the *x*-direction) until position “6”. In this manner, a total of six measured data points along the forming direction of the weld are obtained. These data points can more representatively reflect the residual stress distribution on the weld surface.

Figure 11b shows the comparison results between the simulated values and the measured values. It can be seen that the trend of the measured residual stress values is in good agreement with the simulation results. This comparative analysis verifies the validity of the simulation conducted in this study.

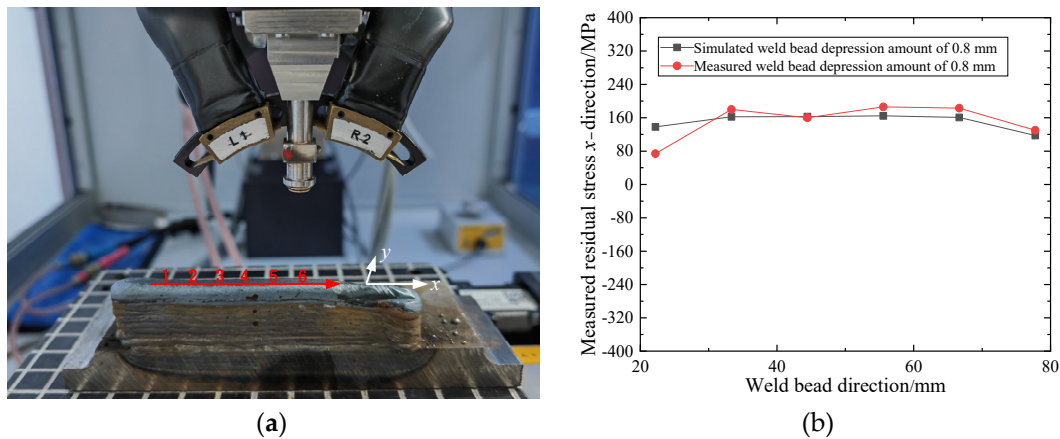


Figure 11. Measured residual stress. (a) Measured residual stress in the x -direction, (b) comparison curve of the simulated and measured values of residual stress for a forward rolling reduction of 0.8 mm.

4. Conclusions

The research findings and conclusions are summarized as follows:

(1) Residual Stress Distribution After Arc Additive Manufacturing

After arc additive manufacturing, the formed part exhibits significant overall residual tensile stress. The residual stress in the x -direction is the highest, making the part more prone to defects such as cracks in the vertical y -direction. Compared to the ends of the model, the residual stress in the middle region of the additive-formed part is relatively stable and evenly distributed.

(2) Impact of Multi-directional Rolling on Residual Stress

After multi-directional rolling, the x -directional stress on the surface of the formed part changes from tensile to significant compressive stress. The average residual stress of the formed part is 317 MPa, which decreases to -62 MPa after rolling, representing a reduction of 119.6%. This result indicates that multi-directional rolling can significantly reduce the risk of defects, such as cracks occurring perpendicular to the x -direction in the formed part. In the thickness direction, the residual compressive stress gradually transitions to tensile stress. At a distance of 12 mm from the surface, the residual stress value is approximately equal to the stress value before rolling. This indicates that the impact of rolling has a specific depth range.

(3) Impact of Rolling on Equivalent Plastic Strain

After rolling, the maximum average increase in the equivalent plastic strain on the surface of the formed part is 0.133. This indicates that the surface microhardness of the formed part is improved after rolling. In the thickness direction, the equivalent plastic strain of the rolled part gradually decreases with increasing depth and reduces to zero at a depth of approximately 10 mm.

Author Contributions: Conceptualization, L.S.; methodology, L.S.; software, L.S.; validation, M.Z.; formal analysis, C.X.; investigation, L.S.; resources, M.Z.; data curation, L.S.; writing—original draft preparation, L.S.; writing—review and editing, L.S. and C.X.; visualization, L.S.; supervision, M.Z.; project administration, C.X.; funding acquisition, M.Z. All authors have read and agreed to the published version of the manuscript.

Funding: This research received no external funding.

Data Availability Statement: The data presented in this study are available on request from the corresponding author.

Conflicts of Interest: The authors declare no conflicts of interest.

References

1. Gibson, I.; Rosen, D.; Stucker, W.B.; Khorasani, M.; Rosen, D.; Stucker, B. *Additive Manufacturing Technologies*; Springer: Berlin, Germany, 2021.
2. Ngo, T.D.; Kashani, A.; Imbalzano, G.; Nguyen, K.T.Q.; Hui, D. Additive Manufacturing (3D Printing): A Review of Materials, Methods, Applications and Challenges. *Compos. Part B Eng.* **2018**, *143*, 172–196. [[CrossRef](#)]
3. Behera, M.P.; Dougherty, T.; Singamneni, S.; Silva, K.D. Selective laser melting of aluminium metal-matrix composites and the challenges. *Mater. Today Proc.* **2020**, *33*, 5729–5733. [[CrossRef](#)]
4. Seely, D.; Bagheri, M.A.; Dickel, D.; Cho, H.E.; Rhee, H.; Horstemeyer, M.F. The Chemistry–Process–Structure Relationships of a Functionally Graded Ti-6Al-4V/Ti-1B Alloy Processed with Laser-Engineered Net Shaping Creates Borlite. *Materials* **2024**, *17*, 3491. [[CrossRef](#)]
5. Heinel, P.; Müller, L.; Körner, C.; Singer, R.F.; Müller, F.A. Cellular Ti-6Al-4V structures with interconnected macro porosity for bone implants fabricated by selective electron beam melting. *Acta Biomater.* **2008**, *4*, 1536–1544. [[CrossRef](#)]
6. Dave, V.R.; Matz, J.E.; Eagar, T.W. Electron beam solid freeform fabrication of metal parts. *Solid Freeform Fabr. Symp.* **1995**, 64–71.
7. Dickens, P.M.; Pridham, M.S.; Cobb, R.C.; Gibson, I.; Dixon, G. Rapid Prototyping Using 3-D Welding. In Proceedings of the 1992 International Solid Freeform Fabrication Symposium, Austin, TX, USA, 3–5 August 1992.
8. Liu, J.; Xu, Y.; Ge, Y.; Hou, Z.; Chen, S. Wire and Arc Additive Manufacturing of Metal Components: A Review of Recent Research Developments. *Int. J. Adv. Manuf. Technol.* **2020**, *111*, 149–198. [[CrossRef](#)]
9. Li, J.; Alkahari, M.; Rosli, N.; Hasan, R.; Ramli, F. Review of Wire Arc Additive Manufacturing for 3D Metal Printing. *Int. J. Autom. Technol.* **2019**, *13*, 346–353. [[CrossRef](#)]
10. Chernovol, N.; Sharma, A.; Tjahjowidodo, T.; Lauwers, B.; Van Rymenant, P. Machinability of Wire and Arc Additive Manufactured Components. *CIRP J. Manuf. Sci. Technol.* **2021**, *35*, 379–389. [[CrossRef](#)]
11. Lopes, J.G.; Machado, C.M.; Duarte, V.R.; Rodrigues, T.A.; Santos, T.G.; Oliveira, J.P. Effect of Milling Parameters on HSLA Steel Parts Produced by Wire and Arc Additive Manufacturing (WAAM). *J. Manuf. Process.* **2020**, *59*, 739–749. [[CrossRef](#)]
12. Zhang, H.; Wang, R.; Liang, L.; Wang, G. HDMR Technology for the Aircraft Metal Part. *Rapid Prototyp. J.* **2016**, *22*, 857–863.
13. Colegrove, P.A.; Martina, F.; Williams, S.W.; Meyer, J. Microstructure of Interpass Rolled Wire plus Arc Additive Manufacturing Ti-6Al-4V Components. *Metall. Mater. Trans. A Phys. Metall. Mater. Sci.* **2015**, *46A*, 6103–6118.
14. Hirtler, M.; Jedynek, A.; Sydow, B.; Sviridov, A.; Bambach, M. A Study on The Mechanical Properties of Hybrid Parts Manufactured by Forging and Wire Arc Additive Manufacturing. *Procedia Manuf.* **2020**, *47*, 1141–1148. [[CrossRef](#)]
15. Bambach, M.; Sizova, I.; Sydow, B.; Hemes, S.; Meiners, F. Hybrid Manufacturing of Components from Ti-6Al-4V by Metal Forming and Wire-Arc Additive Manufacturing. *J. Mater. Process. Technol.* **2020**, *282*, 116689. [[CrossRef](#)]
16. Chao, C.; Lin, S.; Fan, C.; Yang, C.; Zhou, L. Feasibility Analysis of Pulsed Ultrasonic for Controlling the GMAW Process and Weld Appearance. *Int. J. Adv. Manuf. Technol.* **2018**, *97*, 3619–3624.
17. Kalentics, N.; Boillat, E.; Peyre, P.; Gorny, C.; Kenel, C.; Leinenbach, C.; Jhabvala, J.; Logé, R.E. 3D Laser Shock Peening -A New Method for the 3D Control of Residual Stresses in Selective Laser Melting. *Mater. Des.* **2017**, *130*, 350–356. [[CrossRef](#)]
18. Bai, X.; Zhang, H.; Wang, G. Finite Element Analysis of Electromagnetic Force in GMAW Melt Pool Induced by External Magnetic Field. *Trans. China Welding Inst.* **2016**, *37*, 46–50+131.
19. Wang, K.; Zhao, X.; Zhang, K. Experimental research on arc additive Manufacturing based on electromagnetic induction Heating. *J. Huazhong Univ. Sci. Technol. (Nat. Sci. Ed.)* **2022**, *50*, 58–63.
20. Zhao, X.; Wang, Y.; Wang, G.; Li, R.; Zhang, H. Effect of process parameters on stress and strain of hybrid deposition and micro-rolling. *Rapid Prototyp. J.* **2022**, *28*, 490–504. [[CrossRef](#)]
21. Hertel, M.; Rose, S.; Füssel, U. Numerical simulation of arc and droplet transfer in pulsed GMAW of mild steel in argon. *Weld. World* **2016**, *60*, 1055–1061. [[CrossRef](#)]

Disclaimer/Publisher’s Note: The statements, opinions and data contained in all publications are solely those of the individual author(s) and contributor(s) and not of MDPI and/or the editor(s). MDPI and/or the editor(s) disclaim responsibility for any injury to people or property resulting from any ideas, methods, instructions or products referred to in the content.